Brain Tumor Imaging with PET and 2-[Carbon-11]Thymidine

T. Vander Borght, S. Pauwels, L. Lambotte, D. Labar, S. De Maeght, G. Stroobandt and C. Laterre

Departments of Nuclear Medicine, Experimental Surgery, Positron Tomography Laboratory, Neurosurgery and Neurology, University of Louvain Medical School, Brussels, Belgium

Methods: To assess the potential of thymidine for imaging brain tumors, 20 patients with untreated (n = 14) and recurrent (n = 6) supratentorial intracranial tumors were studied with PET by using 2-[^{11}C]thymidine (Tdr), and the results were compared with [^{18}F]fluorodeoxyglucose (FDG) PET data. **Results:** Blood analysis consistently revealed a rapid clearance of the intact Tdr together with the appearance of CO_2/HCO_3^- that, with time, accounted for approximately 70% of the total blood activity. As soon as 10 min after tracer injection, brain images showed a low and homogeneous Tdr distribution over the normal brain structures (cortex-to-blood ratio approximately 1). Visual and quantitative analysis revealed increased Tdr uptake (tumor-to-cortex ratio ≥ 1.2) in 11 of 14 untreated tumors and in 5 of 6 recurrent tumors. No correlation was found between Tdr uptake and tumor grade. In 12 of the 14 untreated tumors, FDG uptake was low (tumor-to-cortex ratio: 0.83 ± 0.79), but a FDG hot spot was visualized in 8 of 10 high-grade and in none of the 4 low-grade tumors. FDG uptake was consistently low in recurrent tumors (tumor-to-cortex ratio: 0.49 ± 0.19), and PET-FDG was negative in 3 of the 6 cases. **Conclusion:** These data indicate the feasibility of brain tumor imaging with Tdr and suggest the potential clinical usefulness of the method in the detection of tumor recurrences. The specificity of the method remains, however, to be investigated.

Key Words: 2-[carbon-11]thymidine; fluorine-18-fluorodeoxyglucose; PET; brain tumors

J Nucl Med 1994; 35:974–982

The development of a method to assess in vivo cellular proliferation would provide an objective tool to measure tumor growth rate and therapeutic response. Cellular proliferation is characterized basically by an increased DNA synthesis that is classically evaluated by measuring ^{3}H- or ^{14}C-labeled thymidine incorporation into DNA on autoradiography or scintillation counting (*1*). The human use of the method is, however, limited by the necessity of tissue sample and radiation hazard.

In brain tumors, glucose use correlates ex vivo with DNA synthesis rate (*2*) and the [^{18}F]fluorodeoxyglucose (FDG) PET method allows noninvasive measurement of tumor grade, prognosis and recurrence (*3–10*). However, FDG uptake involves a process common to both tumor and nontumor tissues. In tumor tissues, FDG uptake is related to inflammatory and neoplastic cells (*11*); in nontumor tissues (i.e., normal brain, abscesses, scar or epileptic focus), the tracer uptake could hamper the interpretation of the tumor's uptake (*12*). These potential drawbacks could be circumvented by developing a more selective tumor tracer. During the last decade, PET imaging with ^{11}C-labeled thymidine (Tdr) was developed to measure noninvasively cellular proliferation (*13,14*). Previous data obtained in a partial hepatectomized rat model showed a correlation between PET-Tdr images and the DNA synthetic rate (*15,16*). The clinical potential of the method in oncology was first evaluated in patients with non-Hodgkin's lymphomas (*17*). In human brain tumors, Hoshino et al. (*18,19*) reported a prognostic value of the labeling index obtained on a surgical sample rapidly after intravenous administration of ^{3}H-thymidine. Other data suggested that thymidine was not taken up by abscesses and could be suitable for monitoring therapy (*20,21*). In this study, the feasibility of Tdr-PET method was investigated in 20 nontreated and recurrent supratentorial tumors, and the potential of the method was assessed by comparison with FDG-PET data.

MATERIALS AND METHODS

Patients

Twenty patients with supratentorial intracranial tumors were investigated (12 male and 8 female patients, mean age 46 yr, range 12–73 yr). Taking into account the resolution of the PET device, only patients with lesions greater than 3 cm on CT scans or MRI were included in the study.

Fourteen patients were referred prior to any surgical and radiotherapeutic treatment with lesions suspicious of tumor on the basis of history, physical examination and radiologic findings, including CT scan and MRI. The biopsy obtained within 1 wk after the PET study revealed eight gliomas and six nonglioma tumors (Table 1).

Six patients entered in this study were suspected of having recurrent intracranial tumors (Table 2). Four patients had undergone surgical resection, combined with radiotherapy in one case. Two patients had only been treated by conventional radiotherapy.

Received Apr. 28, 1993; revision accepted Jan. 26, 1994.

For correspondence or reprints contact: Dr. Stanislas Pauwels, Centre de Médecine Nucléaire, UCL 54.30, Avenue Hippocrate 54, B-1200 Brussels, Belgium, Belgium.

TABLE 1
Patient List with Untreated Gliomateous and Nongliomateous Tumors

Patient no.	Age/Sex	Location of tumor	Final diagnosis*	Grade
Gliomas				
1	73/M	R frontal	Glioblastoma	IV
2	58/M	L frontal	Glioblastoma	IV
3	76/M	R temporal	Glioblastoma	IV
4	32/F	L frontal	Glioblastoma	IV
5	61/M	L corpus callosum	Anaplastic astrocytoma	III
6	28/M	L frontal	Anaplastic astrocytoma	III
7	29/F	L frontal	Anaplastic astrocytoma	III
8	42/F	L temporal	Astrocytoma	II
Nongliomas				
9	32/M	R paracavernous	Meningioma	I
10	54/F	R frontal	Meningioma	I
11	61/M	L parietal	Meningioma	I
12	66/M	R basal ganglia	Primitive lymphoma	IV
13	54/M	L corpus callosum	Primitive lymphoma	IV
14	45/M	L occipital	Adenocarcinoma metastasis	IV

*World Health Organization classification (*22*).
L = left; R = right.

All patients deteriorated clinically and radiologically after initial improvement. PET studies were performed 3.5 yr (median) after the initial intervention. Recurrence was proved in all cases by a surgical or stereotaxic biopsy performed after the PET evaluation. The present study received the approval of the local hospital ethics committee, and patients or their relatives gave oral informed consent.

Radiochemistry

The Tdr was produced by using a three-step synthesis, as previously reported (*23,24*). Briefly, the procedure involved the production of ^{11}C-labeled urea from $^{11}CO_2$, cyclization of ^{11}C-labeled urea with diethylmethylmalate to form 2-[^{11}C]thymine and finally the enzymatic glycosylation of 2-[^{11}C]thymine, leading to Tdr. The radiochemical purity of the high-performance liquid chromatography-isolated material was greater than 99%, and the specific activity averaged 2150 GBq/mmole at the time of injection. Starting from $^{11}CO_2$, the entire Tdr synthesis was achieved in less than 60 min.

The FDG was synthesized according to the method of Hamacher et al. (*25*), and the radiochemical purity of the synthesized material exceeded 95%.

TABLE 2
Summary of Patients with Recurrent Tumors

Patient no.	Age/Sex	Location of tumor	Initial diagnosis*	Treatment	Time from therapy	CT scan	Final diagnosis*
15	18/F	L parietal	Oligoastrocytoma, grade II	Surgery	3.5 yr	Mass effect, enhancement, cavitation	Glioblastoma, grade IV
16	28/M	R frontal	Anaplastic oligoastrocytoma, grade III	Surgery + radiotherapy (54 Gy)	3.5 yr	Light enhancement, cavitation	Anaplastic astrocytoma, grade III
17	46/M	L parietal	Anaplastic astrocytoma, grade III	Surgery	6 yr	Mass effect, light enhancement, cavitation, edema	Anaplastic astrocytoma, grade III
18	12/F	Basal ganglia	No histologic findings	Radiotherapy (60 Gy)	7 mo	Mass effect, light enhancement	Astrocytoma, grade II
19	62/F	L temporal	No histologic findings	Radiotherapy (40 Gy)	14 yr	Mass effect	Oligodendroglioma, grade I
20	69/F	L cerebellopontine angle	Meningioma, grade I	Surgery	3 yr	Mass effect, enhancement	Meningioma, grade I

*World Health Organization classification (*22*).
L = left; R = right.

PET Studies

Following a minimum 4-hr fast (serum glucose 86 ± 26 mg/dl), all patients underwent Tdr and FDG PET studies. After the injection of Tdr, arterial blood samples (1.0 ml) were taken at 15-sec intervals during the first minute and then at 2, 3, 4, 5, 7.5, 10, 15, 20, 25, 30, 45 and 60 min. For the input-curve determination of FDG, 20 to 25 arterial blood samples were withdrawn over a 60-min period, starting immediately after injection.

PET scanning was performed by using an ECAT-III one-ring scanner (in-plane resolution: 5.5–6.0 mm in the central field of view, CTI, Knoxville TN) with a 30-mm collimator aperture, resulting in a slice thickness of 15 mm full width at half maximum (*26*). A weekly calibration of the tomograph versus a well counter was made by measuring a uniform cylindric phantom (diameter 20 cm) filled with a solution of ^{68}Ge.

The patients were positioned in the gantry so that the image plane, oriented parallel to the canthomeatal line, encompassed the tumor region, as determined by the CT scan and MRI. Immediately after intravenous administration of 275 ± 115 MBq of Tdr, PET data were acquired according to the following sequence: 10 × 1 min, 2 × 5 min and, then, depending on the injected dose, from one to four static images until 60 min. After the decay of the residual ^{11}C radioactivity, a 320 ± 80-MBq dose of FDG was administered intravenously and data were acquired beginning 40 min after the injection at the slice level used for the Tdr study. At least two additional FDG scans were acquired at 1 cm on both sides of the initial level. After random coincidence subtraction and normalization, sinograms were corrected for attenuation and isotopic decay. Attenuation correction was carried out by using a contour-finding algorithm and a uniform attenuation coefficient of 0.088 cm^{-1}; the attenuation of the skull and head holder was also taken into account (*27*).

The Tdr and FDG images were first evaluated visually and without knowledge of the biopsy results by at least two readers. The activity in the area corresponding to the CT scan or MRI abnormality, excluding cavitation, was compared with the uptake in the adjacent parenchyma. In FDG studies, gray and white matter were also taken as reference tissues. In patients suspected of recurrence, the FDG scan was considered to be positive when the FDG uptake in the abnormal area was at least similar to that of the white matter.

For quantitative analysis, two regions of interest (ROI) were drawn; the first over the region of highest Tdr tumor uptake on the 17.5-min scan and the other, defined as the control ROI, over a large contralateral gray matter area on the FDG scan. The tumor and control ROIs were further superimposed on all Tdr and FDG images. The ^{11}C radioactivity measured over the ROIs was expressed as the standardized uptake value (SUV) (*28*). To normalize the FDG scan acquired successively at different brain levels, glucose metabolism in the tumor and cortex was estimated by using the autoradiographic model of Sokoloff, adapted for PET by Phelps et al. (*29*). Finally, all the quantitative results of Tdr and FDG metabolism were expressed as a ratio of the tumor-to-contralateral cortex.

Analysis of ^{11}C Blood Radioactivity

The ^{11}C activity was analyzed on each blood sample taken during the Tdr time-course study. A 0.5-ml sample of whole blood was immediately mixed with 2 ml of 3.0 N NaOH to fix all labeled CO_2 as the bicarbonate, whereas another 0.5-ml aliquot was processed to remove CO_2 and bicarbonate by the addition of 2 ml of 2.25 N $HClO_4$. The ^{11}C radioactivity was further determined by using a gamma-counter (Berthold BF-5003, Wilbad, Germany). The total blood radioactivity corrected for the physical decay was expressed as the SUV, whereas the amount of circulating $^{11}CO_2$-$H^{11}CO_3^-$ was expressed as a percentage of the total blood radioactivity.

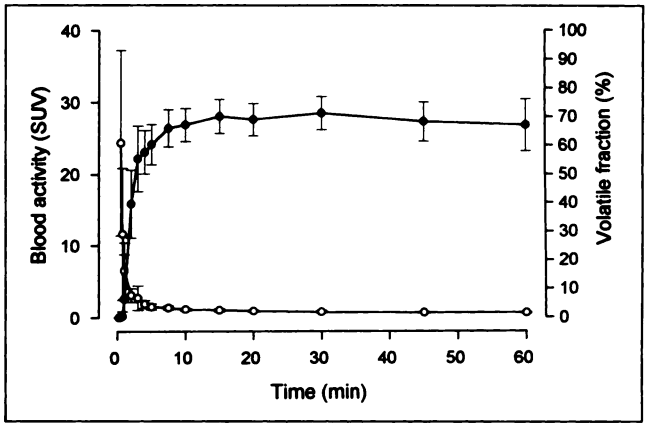

FIGURE 1. Total blood radioactivity (○) (expressed as SUV) and volatile fraction (●) (expressed as a percentage of total blood activity) after Tdr injection (n = 17, mean ± s.d.).

Statistical Analysis

All results were expressed as the mean ± s.d. The data were analyzed using linear-regression analysis and paired and unpaired Student's t-tests, as appropriate.

RESULTS

The Tdr images of normal brain structures obtained within the first minutes following the intravenous injection resembled blood flow images, i.e., the radioactivity was higher over the gray matter areas compared with the white matter areas and maximal over the vascular structures. Thereafter, the activity over the nonproliferating brain structures rapidly redistributed so that the difference between gray and white matter progressively declined. On late images, no notable Tdr uptake was observed, except over the choroid plexus, pituitary gland and subcutaneous regions. At the end of the acquisition, the cortical activity averaged 0.85 SUV, with a 24% interindividual coefficient of variation, and the difference in uptake between gray and white matter did not exceed 5%.

Analysis of the blood radioactivity indicated that during the first minute after Tdr injection, almost all of the radioactive blood content corresponded to nonvolatile material. The volatile fraction increased with time, reaching a plateau level of approximately 70% of total blood activity, 7.5 min after injection (Fig. 1). All tumor Tdr time-activity curves, except those in patients with meningiomas, showed a maximal activity within 5 min, followed by a slow decrease (Fig. 2). Time-activity curves in meningiomas showed an earlier peak, followed by a more rapid decline. After 2.5 min, the cortex time-activity curve had a slow decrease that was parallel to the blood-activity curve. At 17.5 min, the volatile blood activity correlated with the radioactivity measured over the control brain area

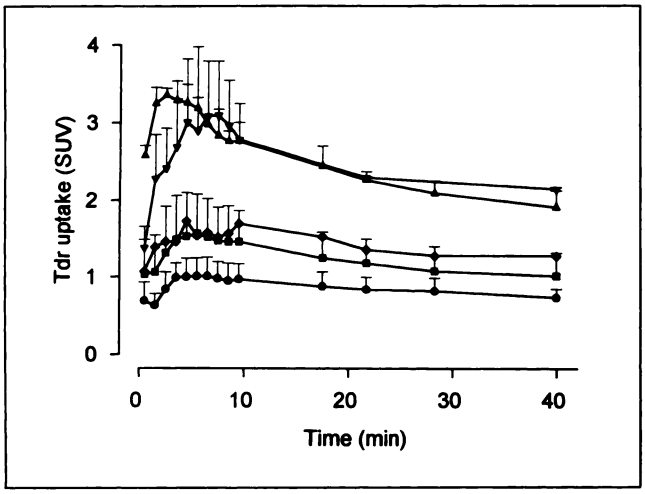

FIGURE 2. Tdr time-activity, expressed as SUV, measured over untreated control (●: n = 9) and brain tumor areas (■: gliomas, n = 4; ▼: primitive lymphomas, n = 2; ◆: adenocarcinoma metastasis, n = 1; ▲: menigiomas, n = 2).

(r = 0.78, p < 0.001) with a slope nonstatistically different from 1 (0.97 ± 0.20).

In the group of untreated tumors, visual examination of the 17.5-min Tdr scan revealed, in 11 of 14 cases, a hot spot in the tumor area (Table 3 and Fig. 3). An increase in acquisition time, when possible, did not improve the tumor-to-background contrast. Tumor uptake was similar to the surrounding tissue in three cases: two rim-shaped glioblastomas with large central necrotic areas and one low-grade astrocytoma. The highest and the most homogeneous tracer accumulation was observed in nongliomatous tumors. The quantitative Tdr data, expressed as the SUV, correlated with the visual data in that the three lowest cortex-to-tumor ratios were found in the three patients with no visible focal uptake. Significantly increased tracer uptake was present in the nontreated tumors compared with that in the control area of brain (1.64 ± 0.65 versus 0.86 ± 0.16 SUV, p < 0.001). Considering the entire group of untreated tumors, no correlation was found between Tdr uptake and tumor grade, and this was because of the high Tdr uptake observed in the low-grade meningiomas. At the same slice level, the FDG images revealed a tumor metabolism that was higher than the contralateral cortex in two patients, similar in one patient, intermediate (higher than white but lower than gray matter) in five patients and equal or lower than the white matter in 6 of 14 patients. Compared with the surrounding parenchyma, increased glucose metabolism, appearing as a hot focus, was present in 8 of

TABLE 3
2-[Carbon-11]Thymidine and Fluorine-18-Fluorodeoxyglucose PET Findings

			Tdr			FDG		
						Visual evaluation*		
Patient no.	Final diagnosis	Grade	Visual focus	Tumor SUV	Tumor/ Cortex	Focus	Uptake	Tumor/ Cortex
Nontreated gliomas								
1	Glioblastoma	IV	–	1.04	1.08	–†	~white	0.56
2	Glioblastoma	IV	+	1.46	1.50	+	>white	0.61
3	Glioblastoma	IV	+	1.13	1.20	+	>white	0.45
4	Glioblastoma	IV	–	0.68	1.05	–†	~white	0.39
5	Anaplastic astrocytoma	III	+	1.62	1.34	+	>white	0.54
6	Anaplastic astrocytoma	III	+	1.03	1.20	–	~white	0.65
7	Anaplastic astrocytoma	III	+	1.31	1.70	–	>white	0.76
8	Astrocytoma	II	–	0.90	1.06	–	<white	0.36
Nontreated nongliomas								
9	Meningioma	I	+	2.27	3.50	–	<white	0.41
10	Meningioma	I	+	2.63	3.11	–	<white	0.28
11	Meningioma	I	+	2.36	2.21	–	>white	0.74
12	Primitive lymphoma	IV	+	2.62	2.61	+	>gray	3.44
13	Primitive lymphoma	IV	+	2.29	3.29	+	>gray	1.56
14	Adenocarcinoma metastasis	IV	+	1.53	2.03	+	~gray	0.84
Recurrences								
15	Glioblastoma	IV	+	0.92	1.37	–	<white	0.24
16	Anaplastic astrocytoma	III	+	1.32	1.50	+	~gray	0.73
17	Anaplastic astrocytoma	III	–	0.77	0.84	–	<white	0.31
18	Astrocytoma	II	+	1.40	1.31	–	~white	0.55
19	Oligodendroglioma	II	+	0.74	1.31	–	~white	0.70
20	Meningioma	I	+	6.94	7.18	–	<white	0.41

*Tumor FDG uptake was described as a focus when the lesion appeared as a hot spot compared with the surrounding tissue, and then tumor uptake was also visually compared with gray and white matter uptake (higher: >; similar: ~; lower: <).

†A visual focus was observed at a slice adjacent to the Tdr slice level.

10 high-grade tumors (6 at the Tdr slice level and only 2 visible on adjacent slices) and in none of the four low-grade tumors. In all untreated tumors, except the two high-grade lymphomas, the quantitative analysis indicated a decrease in glucose metabolism compared with the opposite gray matter region (mean tumor-to-cortex ratio 0.83 ± 0.79 for n = 14). The FDG tumor-to-cortex ratio did not correlate with the tumor grade. Only two of the four low-grade tumors had a lower tumor-to-cortex ratio compared with the 10 high-grade tumors.

Tdr uptake was observed in all recurrent tumors (Fig. 4). In five of six cases, the tumor-to-cortex ratio was higher than 1.2 (mean 2.02 ± 2.22 for n = 6), allowing a clear visualization of the recurrence. In none of the 6 patients, was there an elevated FDG uptake (mean tumor-to-cortex ratio 0.49 ± 0.19). In three patients, the FDG study was negative, i.e., the uptake in the suspected area was lower compared with that in the surrounding tissue. Recurrence could be suspected in two patients on the basis of FDG uptake similar to the white matter. In one case, a hot spot was seen at the margin of the lesion but was not distinguishable from the adjacent cortex.

Interestingly, in the intracerebral tumors (i.e., all treated and untreated cases, except meningiomas), a positive correlation was found between Tdr uptake, expressed as SUV, and FDG tumor uptake, expressed as the ratio tumor-to-control ratio ($r = 0.84$, $p < 0.001$, $n = 16$). Similarly, Tdr tumor-to-control ratios were correlated with FDG tumor-to-control ratios ($r = 0.74$, $p < 0.001$, $n = 16$).

DISCUSSION

The present clinical study demonstrated that 2-[^{11}C]thymidine can be used to image brain tumors and extended the preliminary reports of the potential of PET-Tdr in brain tumor assessment (*30,31*). In all investigated tumors, uptake of the tracer was observed, and in 80% of the patients, the tumor appeared as an area of increased activity compared with the surrounding structures. Besides this diagnostic potential, the principal finding of the study was that, in patients with recurrent tumors, PET-Tdr provided a better visualization of the tumor than did FDG imaging.

During the first minutes after injection, Tdr was rapidly cleared from the circulation. The initial brain images resembled blood flow images and were therefore not useful for functional imaging. Very rapidly, however, the activity over nonproliferating brain structures underwent a redistribution; after 10 min, gray and white matter uptake became homogeneous and, thus, blood flow independent. Given the limitations imposed by the short half-life of ^{11}C and the maximum dose available in the diagnostic procedure, these data suggest that images acquired during the first 20 min postinjection would be adequate for brain tumor imaging. At 17.5 min, the tumor-to-background ratio was >1 in 95% of the patients imaged with Tdr. As a result of the low and homogeneous uptake over gray and white matter structures, the tumor was clearly visualized when the target-to-nontarget activity reached 1.2. Despite a higher tumor uptake of FDG compared with that of Tdr, the visualization of the tumor was less clear on FDG images because of heterogeneous background activity. Normal brain imaged with FDG shows high activity in gray matter and low activity in white matter. The tumor may be therefore easily confused with normal structures, particularly when it invades the gray matter for a high-grade glioma (Patient 16) and the white matter for a low-grade glioma (Patient 8). However, a reduction in glucose use in the area contiguous to the neoplasm, partially related to edema and deafferentation, in some cases, improved the visualization of the tumor area (Patient 14).

Several studies document the usefulness of PET-FDG for differentiating recurrent tumor from necrosis after therapy (*9,10*). Potentially, the accuracy of the method remains questionable because increased glucose metabolism may occur in other conditions frequently encountered in the differential diagnosis of brain lesions, i.e., inflammation, infection or seizure activity (*11,12*). Also, the recognition of recurrent tumor tissue may be hampered by the physiologic FDG uptake in normal brain structures. In the current study, an area of increased FDG activity, compared with the surrounding tissue, was found in only one patient. Defining a positive test result by an uptake at least similar to the white matter increased the sensitivity to 50%. By contrast, PET using Tdr demonstrated tumor uptake in all cases and a hot spot in five of the six patients. These results are in agreement with the preliminary findings of Conti et al. (*30*) who reported positive PET-Tdr findings in four patients with biopsy-proven intracranial recurrences. Although other groups showed that a negative FDG image does not rule out tumor recurrence, they generally reported an overall accuracy of the method in the diagnosis of recurrence that was higher than 80% (*32–35*). The authors have no evident explanation for the relatively low sensitivity observed with FDG in the present study. Several points, including scanning techniques, image interpretation and tumor characteristics, could be responsible for the difference between these results and those reported by other centers.

In some cases, especially in the presence of cavitation, the viable tissue may be confined to a focus localized in the surrounding rim. Because of limited size, such a recurrent tumor may be difficult to detect and might require that the suspected area be completely encompassed by the PET images. Whereas Tdr acquisition was performed at a single scan position, at least five adjacent FDG images of 15-mm resolution were obtained in all patients suspected of recurrence; even in the case of a rim-shaped lesion, therefore, a hypermetabolic area would have been recognized. Interestingly, two of the three patients with evident cavitation on the CT scan had false-negative FDG study results. The criteria for a positive test result vary from author to author in that the tissue reference to which the tumor's metabolism is compared is either the contralateral region (*9*) or the immediately adjacent tissue (*32*). In their study of patients

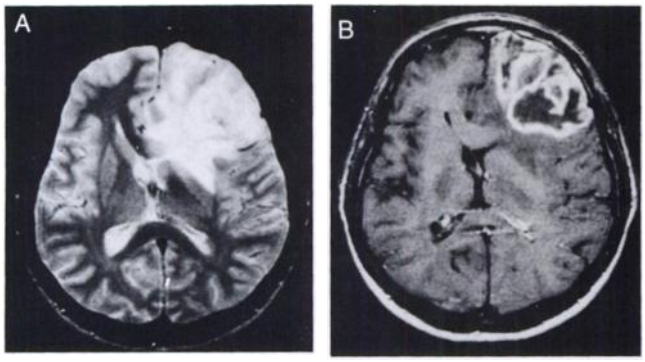

FIGURE 3. Patient with an untreated anaplastic astrocytoma, grade III (Patient 2). (A) MRI T2-weighted image shows two rim-shaped left frontal lesions with a mass effect and brain edema. (B) MRI T1-weighted image with gadolinium shows an intense BBB disruption. (C, left) On the 17.5-min image, intense accumulation of Tdr in the anterior part of the lesion, adjacent to a defect related to a necrotic area. Note the low and homogeneous uptake in normal brain structures and Tdr uptake over the choroid plexus and subcutaneous regions. (C, right) FDG-PET image shows a glucose metabolic rate intermediate between that of gray and white matter and a focus compared with that of the surrounding tissue.

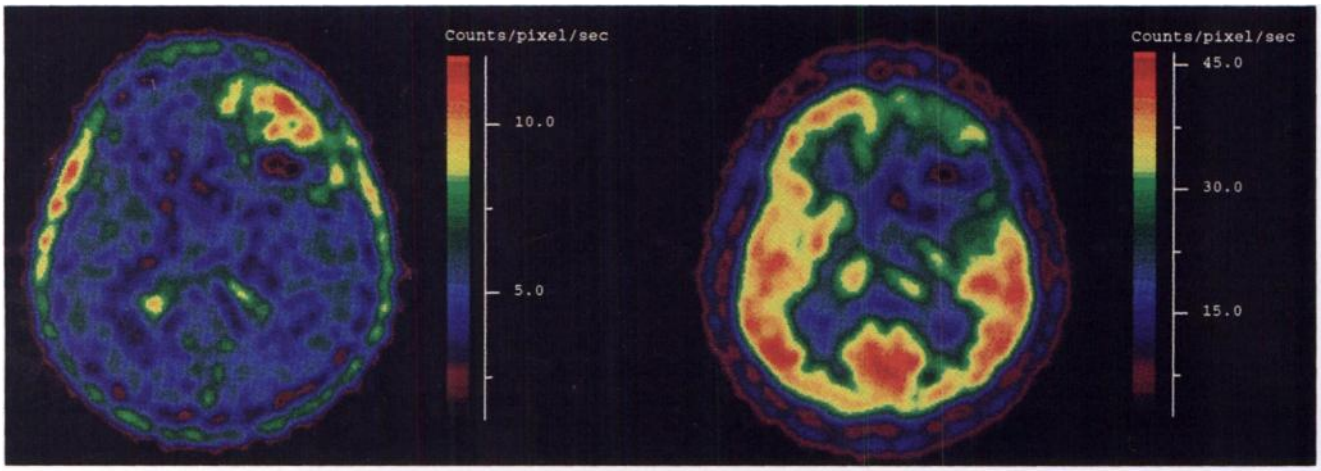

with suspected tumor recurrence, Di Chiro et al. (*10*) reported PET FDG findings to be positive for recurrence in the presence of a visually distinct hypermetabolic focus within the suspected lesion. It should be stressed that, in the six patients studied in the present report, gray, white and adjacent tissues were used as references. The best sensitivity was obtained when the tumor's uptake was compared with the lowest metabolic reference tissue, namely the white matter. The histologic results obtained after the PET study revealed low-grade tumors in three of six cases of recurrence, which represents a high percentage of low-grade tumors compared with the series reported by the other centers. However, the difference in the degree of malignancy cannot solely explain the low sensitivity in this study because the positivity of the PET-FDG findings was not related to the grade of the recurrent tumor (two of three low-grade and one of three high-grade tumors were FDG positive).

After the initial report of Di Chiro et al. (*10*), FDG was extensively used for brain tumor grading and the assessment of prognosis (*5–8*). Different methodologic approaches, quantitative or qualitative, were proposed. The use of absolute quantification of the tumor's glucose metabolism, based on a tracer kinetic method, still remains open to question (*36*). Therefore, in addition to the kinetic evaluation, most investigators also express the tumor's metabolism relative to that of a reference tissue. Alternatively, the tumor's metabolism may be estimated qualitatively by a visual inspection of the images, searching for a hot spot that characterizes high-grade tumors. Because it was not always possible to find a large white matter area at the tumor slice level, a large contralateral gray matter area was used in the present study as the reference. By contrast with previous reports (*3,5*), but in agreement with other investigators (*37,38*), it was found that 90% of tumors had a relatively low tumor-to-control ratio that did not correlate with the tumor grade in the current study. However, by visual examination, a hypermetabolic area contrasting with the surrounding parenchyma was found in most high-grade tumors and in none of the low-grade untreated lesions.

Although Tdr and FDG correlated in patients with intracerebral lesions (treated and untreated), the overall results suggest that Tdr uptake is not a good marker of the degree of malignancy. This lack of correlation between uptake and tumor grade could be a result of the histologic heterogeneity of the tumors and also the small number of low-grade tumors in this series. However, the discrepancy between FDG and Tdr uptake observed in low-grade meningiomas raises questions regarding the significance of increased Tdr uptake in nonmalignant nonintracerebral tumors and, more particularly, in regard to the factors that could influence the tumor uptake.

Information obtained with Tdr and PET must be interpreted in the light of the thymidine metabolic pathways taking place inside and outside the brain. When given intravenously, Tdr is rapidly cleared from the circulation and, in most organs, the initial distribution correlates with

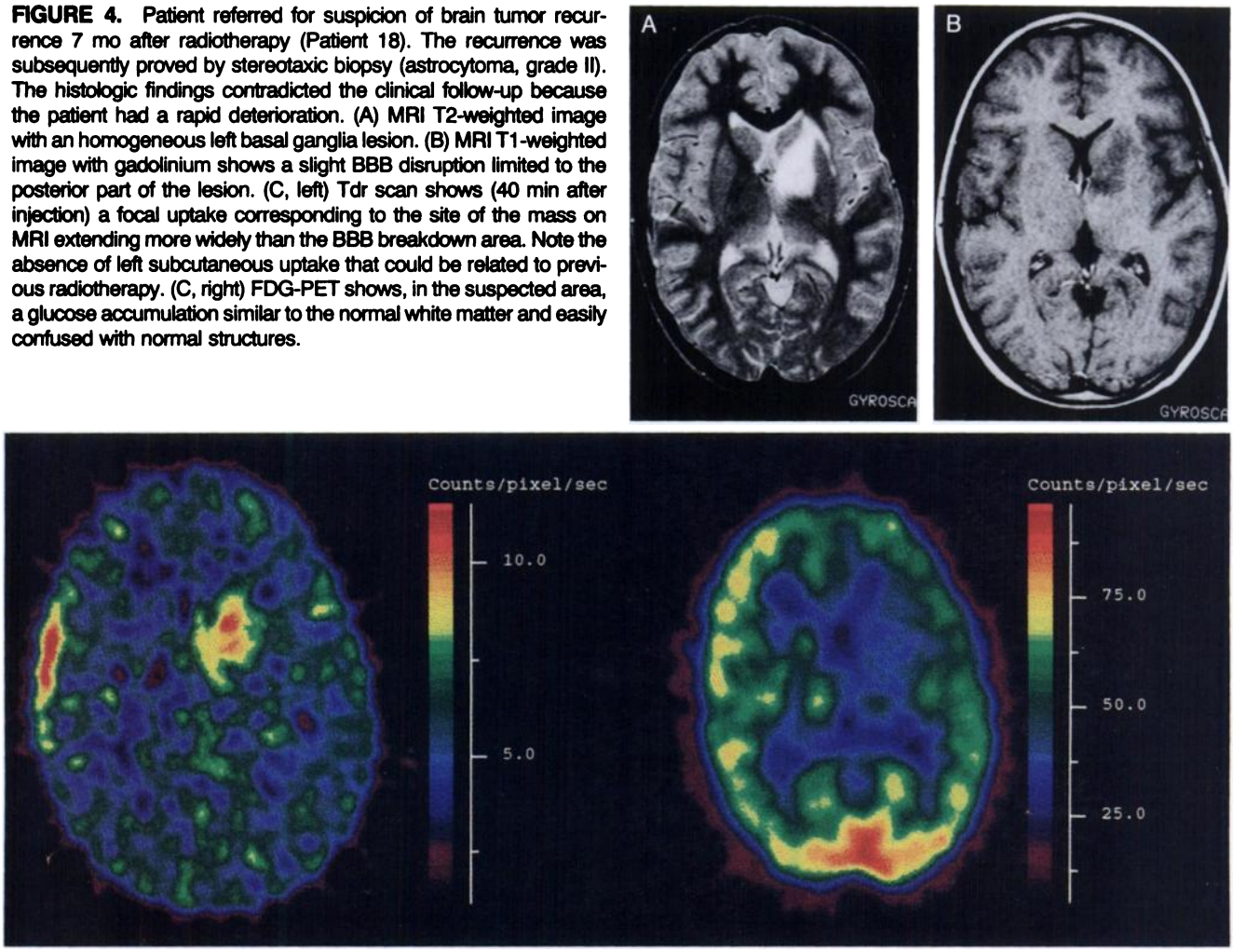

FIGURE 4. Patient referred for suspicion of brain tumor recurrence 7 mo after radiotherapy (Patient 18). The recurrence was subsequently proved by stereotaxic biopsy (astrocytoma, grade II). The histologic findings contradicted the clinical follow-up because the patient had a rapid deterioration. (A) MRI T2-weighted image with an homogeneous left basal ganglia lesion. (B) MRI T1-weighted image with gadolinium shows a slight BBB disruption limited to the posterior part of the lesion. (C, left) Tdr scan shows (40 min after injection) a focal uptake corresponding to the site of the mass on MRI extending more widely than the BBB breakdown area. Note the absence of left subcutaneous uptake that could be related to previous radiotherapy. (C, right) FDG-PET shows, in the suspected area, a glucose accumulation similar to the normal white matter and easily confused with normal structures.

relative perfusion measurements (*39*). Thymidine is not readily transported across the blood-brain barrier (BBB), and although the choroid plexus can concentrate and release Tdr, the effective transport of Tdr from the blood to the brain by the cerebrospinal fluid is negligible, if any, after a bolus injection (*40–42*). Thus, following the injection of Tdr, the initial activity measured over the normal brain structures corresponds to the blood activity present in the vasculature, which is higher in the gray than in the white matter, and is variable over the tumor area.

The diffusion or transport of Tdr across the blood-to-tumor barrier (BTB) constitutes a prerequisite for the accumulation of the molecule in the tumor. Once inside the cell, Tdr can be degraded, giving rise to labeled metabolites, or trapped, and the rate-limiting step for Tdr accumulation is phosphorylation, which constitutes the first step leading to Tdr incorporation into DNA. Thus, besides increased DNA synthesis, the processes that could modulate the Tdr signal in a brain tumor include flow, BTB permeability and the accumulation of labeled metabolites. In time-course studies, the tumor's activity observed on the first images depends on the blood delivery and the degree of BTB permeability. Several groups studying BTB disruption with PET reported ^{68}Ga-EDTA accumulation in glioblastomas, anaplastic astrocytomas and meningiomas but not in low-grade astrocytomas (*43–45*). On the basis of these results, it would be expected that Tdr does not accumulate in low-grade gliomas. Interestingly, the tumor-to-cortex uptake was increased in three cases of low-grade gliomas, and in two of them, a clear hot spot was found over the tumor area, indicating that Tdr is delivered to the tumor, even when the alterations of the BTB are expected to be minimal. Although BBB integrity was not specifically evaluated in the present study, a comparison of CT scans and Tdr images also suggests that Tdr was not mainly a marker of BBB disruption. In some patients with major contrast enhancement on CT scan, the Tdr uptake was low compared with others who had no evident CT scan signs of BBB damage (i.e., Patient 18, Fig. 4). The idea that Tdr is related to nucleic acid metabolism and not solely to an impairment of BBB is also supported by a recent autoradiographic study comparing ^{14}C-labeled aminoisobutyric acid, ^{18}F-labeled fluoro-2′-deoxyuridine and ^{14}C-labeled thymidine in rat brain tumors (*46*). It is clear that further PET studies are needed to evaluate the relationship between BBB damage and Tdr uptake.

Another problem to consider in PET studies is the retention of labeled metabolites. In the case of Tdr, which is labeled in the ring 2 position, thymine, dihydrothymine, beta-ureidoisobutyric acid and CO_2/HCO_3^- constitute the major labeled metabolites. The thymidine that does not follow the incorporation pathway is rapidly degraded to thymine by Tdr phosphorylase, which is extremely widespread and is found in many tissues, including the brain. Subsequent degradation that gives rise finally to labeled CO_2 mainly occurs in the liver, kidneys and spleen from which the degraded products may recirculate (*1*). Thymine crosses the BBB poorly after a bolus injection, if not at all (*40*). The constant 70% volatile blood activity within the first minutes after injection and the similar activity found between gray matter and blood activity suggests that $^{11}CO_2/H^{11}CO_3^-$ accounts for the most part of the normal brain uptake.

Recent animal studies indicate that the contribution of $^{11}CO_2$ to PET images may not be disregarded because of its rapid elimination through the lungs (*47*). After the injection of labeled CO_2/HCO_3^- in dogs, 50% of the injected dose was still retained in the body and could therefore contribute to the PET signal. By contrast with normal BBB, the altered blood-to-tumor barrier could allow the diffusion of the labeled intermediate metabolites into the tumor tissue. The development of a kinetic model and the measurement of the activity really incorporated into DNA should allow a determination of the diffusion of the intermediate labeled metabolites into the tumor tissue. If the contribution to the PET signal of labeled metabolites other than CO_2/HCO_3^- could be neglected, parallel measurement of the tumor pH and Tdr uptake would isolate the true DNA synthetic pathway (*48,49*).

Although the number of patients investigated was relatively small, the present study shows the feasibility of the PET-Tdr method for imaging intracranial tumors. In spite of a lower absolute tumor targeting in comparison with FDG, the tumor lesions were better visualized with Tdr because of a low homogeneous background. Taking into account the present results obtained in patients suspected of having tumor recurrences and recent ex vivo studies demonstrating a decline of Tdr after radiotherapy (*21*), a potential clinical interest of the method could be in monitoring therapy. Although preliminary data obtained in rats showed no Tdr uptake in brain abscesses (*20*), the specificity of the method remains to be confirmed in clinical studies of nontumor lesions. Future studies should also address the correction of the PET-Tdr signal to obtain a true proliferation index. The data from the current study suggest that the assessment of factors (i.e., blood flow, blood volume and labeled metabolites) that may contribute to the PET images could be approached by using Tdr labeled in the ring 2 position, which is rapidly degraded to labeled CO_2, and by performing time-course studies associated with analyses of blood activity. A major issue that has to be resolved is whether the influence of the BBB disruption on the brain tumor Tdr signal can be predicted by the use of a specific BBB tracer.

ACKNOWLEDGMENTS

The authors thank Drs. J. M. Brucher, A. Bol and C. Michel for their assistance. The help of Dr. R. Wahl (University of Michigan, Ann Arbor, MI) in the revision of this article was greatly appreciated. This work was supported by grant 3.4560.87 from the Fund for Medical Scientific Research (Belgium).

REFERENCES

1. Cleaver JE. Thymidine metabolism and cell kinetics. In: *Frontiers of biology, volume 6.* Amsterdam: North-Holland Publishing; 1967.
2. Watanabe A, Tanaka R, Takeda N, Washiyama K. DNA synthesis, blood flow, and glucose utilization in rat brain tumors. *J Neurosurg* 1989;70:86–91.
3. DiChiro G, DeLaPaz RL, Brooks RA, et al. Glucose utilization of cerebral gliomas measured by 18-F-fluoro-deoxyglucose and positron emission tomography. *Neurology* 1982;32:1323–1329.
4. Mineura K, Yasuda T, Kowada M, et al. PET evaluation of histological malignancy in gliomas using 15-oxygen and 18-fluorine-fluorodeoxyglucose. *Neurol Res* 1986;8:164–168.
5. DiChiro G, Hatazawa J, Katz DA, Rizzoli HV, DeMichele DJ. Glucose utilization by intracranial meningiomas as an index of tumor aggressivity and probability of recurrence: a PET study. *Radiology* 1987;164:521–526.
6. Patronas NJ, DiChiro G, Kufta C, et al. Prediction of survival in glioma patients by means of PET. *J Neurosurg* 1985;62:816–822.
7. DiChiro G. Positron emission tomography using [^{18}F]fluorodeoxyglucose in brain tumors: a powerful diagnostic and prognostic tool. *Invest Radiol* 1986;22:360–371.
8. Alavi JB, Alavi A, Chawluk J, et al. Positron emission tomography in patients with glioma: a predictor of prognosis. *Cancer* 1988;62:1074–1078.
9. Patronas NJ, DiChiro G, Brooks RA, et al. Fluorine-18-fluorodeoxyglucose and positron emission tomography in evaluation of radiation necrosis of the brain. *Radiology* 1982;144:885–889.
10. Di Chiro G, Oldfield E, Wright DC, et al. Cerebral necrosis after radiotherapy and/or intraarterial chemotherapy for brain tumors: PET and neuropathological studies. *AJNR Am J Neuroradiol* 1987;8:1083–1091.
11. Kubota R, Yamada S, Kubota K, et al. Intratumoral distribution of fluorine-18-fluorodeoxyglucose in vivo: high accumulation in macrophages and granulation tissues studied by microautoradiography. *J Nucl Med* 1992;33:1972–1980.
12. Sasaki M, Ichiya Y, Kuwabara Y, et al. Ringlike uptake of [^{18}F]FDG in brain abscess: a PET study. *J Comput Assist Tomogr* 1990;14:486–487.
13. Christman D, Crawford EJ, Friedkin M, Wolf AP. Detection of DNA synthesis in intact organisms with positron-emitting [methyl-^{11}C]thymidine. *Proc Natl Acad Sci USA* 1972;69:988–992.
14. Crawford EJ, Christman D, Atkins H, Freidkin M, Wolf AP. Scintigraphy with positron-emitting compounds—I. Carbon-11-labeled thymidine and thymidylate. *Int J Nucl Med Biol* 1978;5:61–69.
15. Vander Borght T, Lambotte L, Pauwels S, Dive C. Uptake of thymidine labeled on carbon 2: a potential index of liver regeneration by positron emission tomography. *Hepatology* 1990;12:113–118.
16. Vander Borght T, Lambotte L, Pauwels S, et al. Noninvasive measurement of liver regeneration with PET and 2-[^{11}C]thymidine. *Gastroenterology* 1991;101:794–799.
17. Martiat P, Ferrant A, Labar D, et al. In vivo measurement of carbon-11 thymidine uptake in non-Hodgkin's lymphoma using positron emission tomography. *J Nucl Med* 1988;29:1633–1637.
18. Hoshino T, Wilson CB. Cell kinetic analyses of human malignant brain tumors (gliomas). *Cancer* 1979;44:956–962.
19. Hoshino T. A commentary on the biology and growth kinetics of low-grade and high-grade gliomas. *J Neurosurg* 1984;61:895–900.
20. Grossman SA, Eller S, Dick J, Burch PA, Yang K. Thymidine, leucine and 2-deoxyglucose. Incorporation in brain tumors and abscesses: a quantitative autoradiographic study with implications for PET scans [Abstract]. *Ann Proc Am Assoc Cancer Res* 1988;29:516.
21. Kubota K, Ishiwata K, Kubota R, et al. Tracer feasibility for monitoring tumor radiotherapy: a quadruple tracer study with fluorine-18-fluorodeoxyglucose or fluorine-18-fluorodeoxyuridine, L-[methyl-^{14}C]-methionine, [6-^{3}H]thymidine, and gallium-67. *J Nucl Med* 1991;32:2118–2123.
22. Zülk KJ. Histological typing of tumors of the central nervous system. In:

International histological classification of tumors, no. 21. Geneva: World Health Organization; 1979:17–67.
23. Vander Borght T, Pauwels S, Lambotte L, De Saeger C, Beckers C. Synthesis of 2-[^{14}C]thymidine: a potential route for 2-[^{11}C]thymidine. *J Labelled Comp Radiopharm* 1990;28:819–822.
24. Vander Borght T, Labar D, Pauwels S, Lambotte L. Production of 2-[^{11}C]thymidine for quantification of cellular proliferation with PET. *Appl Radiat Isotopes* 1991;41:103–104.
25. Hamacher K, Coenen HH, Stöcklin G. Efficient stereospecific synthesis of non-carrier added 2-[^{18}F]-fluoro-2-deoxy-D-glucose using aminopolyether supported nucleophilic substitution. *J Nucl Med* 1986;27:235–238.
26. Hoffman EJ, Phelps ME, Huang SC, et al. Dynamic, gated and high resolution imaging with the ECATIII. *IEEE Trans Nucl Sci* 1986;33:452–455.
27. Michel C, Bol A, De Volder AG, Goffinet AM. On-line brain attenuation correction in PET: towards a fully automated data handling in a clinical environment. *Eur J Nucl Med* 1989;15:712–718.
28. Woodard HQ, Bigler RE, Freed B, Russ G. Expression of tissue isotope distribution. *J Nucl Med* 1975;16:958–959.
29. Phelps ME, Huang SC, Hoffman EJ, et al. Tomographic measurement of local cerebral glucose metabolic rate in humans with [F-18]-2-fluoro-2-deoxy-D-glucose: validation of the method. *Ann Neurol* 1979;6:371–388.
30. Conti PS, Grossman SA, Wilson AA, et al. Brain tumor imaging with C-11 labeled thymidine and PET [Abstract]. *Radiology* 1990;197P:234.
31. Vander Borght T, Pauwels S, Lambotte L, et al. PET study of human cerebral malignancy with 2-[^{11}C]thymidine and [^{18}F]FDG [Abstract]. *Eur J Nucl Med* 1991;18:540.
32. Doyle WK, Budinger TF, Valk PE, Levin VA, Gutin PH. Differentiation of cerebral radiation necrosis from tumor recurrence by [^{18}F]FDG and ^{82}Rb and positron emission tomography. *J Comput Assist Tomogr* 1987;11:563–570.
33. Ogawa T, Kanno I, Shishido F, et al. Clinical value of PET with ^{18}F-fluorodeoxyglucose and L-methyl-^{11}C-methionine for diagnosis of recurrent brain tumor and radiation injury. *Acta Radiol* 1991;32:197–362.
34. Valk PE, Budinger TF, Levin VA, et al. PET of malignant cerebral tumors after interstitial brachytherapy: demonstration of metabolic activity and correlation with clinical outcome. *J Neurosurg* 1988;69:830–838.
35. Glantz MJ, Hoffman JM, Coleman RE, et al. Identification of early recurrence of primary central nervous system tumors by [^{18}F]fluorodeoxyglucose positron emission tomography. *Ann Neurol* 1991;29:347–355.
36. DiChiro G. PET quantitation: blessing and curse. *J Nucl Med* 1988;29:1603–1604.
37. Tyler JL, Diksic M, Villemure JG, et al. Metabolic and hemodynamic evaluation of gliomas using positron emission tomography. *J Nucl Med* 1987;28:1123–1133.
38. Heiss WD, Heindel W, Herholz K, et al. Positron emission tomography of fluorine-18-deoxyglucose and image-guided phosphorus-31 magnetic resonance spectroscopy in brain tumors. *J Nucl Med* 1990;31:302–310.
39. Shields AF, Larson SM, Grunbaum Z, Graham MM. Short-term thymidine uptake in normal and neoplastic tissues: studies for PET. *J Nucl Med* 1984;25:759–764.
40. Cornford EM, Oldendorf WH. Independent blood-brain-barrier transport systems for nucleic acid precursors. *Biochim Biophys Acta* 1975;394:211–219.
41. Spector R. Thymidine accumulation by choroid plexus in vitro. *Arch Biochem Biophys* 1980;205:85–93.
42. Pardridge WM. Recent advances in blood-brain-barrier transport system. *Annu Rev Pharmacol Toxicol* 1988;28:25–39.
43. Mosskin M, von Holst H, Ericson K, Noré G. The blood-tumor-barrier in intracranial tumor studied with x-ray computed tomography and positron emission tomography using ^{68}Ga-EDTA. *Neuroradiology* 1986;28:259–263.
44. Wienhard K, Herholz K, Coenen HH, et al. Increased amino acid transport into brain tumors measured by PET of L-[2-^{18}F]fluorothyrosine. *J Nucl Med* 1991;32:1338–1346.
45. Ericson K, Lilja A, Bergstrom M, et al. Positron emission tomography with [^{11}C]methyl-L-methionime, [^{11}C]D-glucose, and [^{68}Ga]EDTA in supratentorial tumors. *J Comput Assist Tomogr* 1985;9:683–689.
46. Tsurumi Y, Kameyama M, Ishiwata K, et al. ^{18}F-fluoro-2′-deoxyuridine as a tracer of nucleic acid metabolism in brain tumors. *J Neurosurg* 1990;72:110–113.
47. Shields AF, Graham MM, Kozawa SM, et al. Contribution of labeled carbon dioxide to PET imaging of C-11-labeled compounds. *J Nucl Med* 1992;33:581–584.
48. Brooks DJ, Lammertsma AA, Beaney RP, et al. Measurement of regional cerebral pH in human subjects using continuous inhalation of $^{11}CO_2$ and positron emission tomography. *J Cereb Blood Flow Metab* 1984;4:458–465.
49. Buxton RB, Wechsler LR, Alpert NM, et al. Measurement of brain pH using $^{11}CO_2$ and positron emission tomography. *J Cereb Blood Flow Metab* 1984;4:8–16.